CHAPTER 185

SAND TRANSPORT UNDER GROUPING WAVES

Shinji Sato[1]

Abstract

Laboratory experiments as well as numerical modeling were conducted for sand transport under non-breaking grouping waves. Experiments showed that the direction of net transport of fine sand was onshore under grouping waves although it was offshore under monochromatic waves with equivalent wave height. It was also revealed that the long wave bounded to wave group plays an important role in particular for suspended load. A numerical model was developed on the basis of the second-order Stokes wave theory and one-dimensional diffusion equation of sand concentration. The validity of the model was confirmed with experimental data.

1. INTRODUCTION

In order to develop a proper model of sediment transport under random waves, we have to understand the mechanism of sand transport under wave groups since waves in nature usually contain various waves groups. Wave grouping may influence the amount and the direction of sand movement through direct action of a series of large waves as well as the interaction of short- and long-wave component involved in the group. For example, Shi and Larson (1984) suggested that the direction of sand transport under grouping waves will be offshore because the bound long wave will induce offshore flow under large waves when more sediment is likely to be suspended. The check of this suggestion by laboratory experiments is one motivation of the present study.

The present study aims at understanding the effect of the grouping of non-breaking waves on local sand movement through extensive laboratory experiments

[1] Assoc. Prof., Dept. of Civil Eng., Yokohama National Univ., Hodogaya-Ku, Yokohama 240, Japan

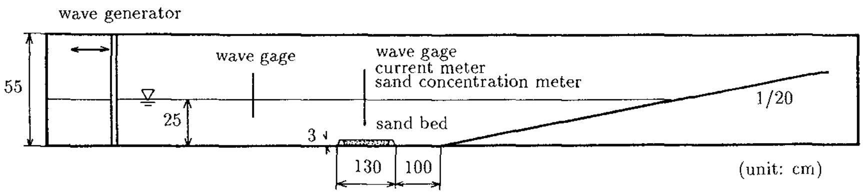

Fig. 1 Experimental setup

and developing a predictive model of sand transport rate under grouping waves. Particular attention will be paid on the effects of long wave and the number of waves in a group on the direction of suspended sediment flux.

2. LABORATORY EXPERIMENTS

A series of experiments were performed in a wave flume in which monochromatic waves and bichromatic grouping waves were generated. Figure 1 shows the layout of experiments. A sand tray was placed at constant depth region where sand was filled to make an initially flat bed. Two kinds of sand with median diameter D =0.02cm and 0.07cm were used as bed materials. Water surface profile and near-bottom velocity at 5cm above the bottom were measured at the center of the tray by a wave gage and a ultrasonic current meter. In one run of experiments with fine sand ($H_1 = H_2 = 6$cm, $T_1 = 1.0$s, $T_2 = 1.175$s), suspended sand concentration was also measured by an optical concentration meter at various elevations above a ripple crest and a trough. Waves were generated until significant sand transport was observed in the tray. The time duration of wave action in each run of experiments ranged from 20 to 50 minutes. Sand movement due to wave action was recorded by a VTR camera. After each run of experiments, the geometry of sand ripples was measured and a thin plate was inserted at the center of the tray. The sand on the left side and the right side of the tray was collected separately. The net sand transport rate at the center of the tray was estimated from the mass difference of dried sand in both sides of the tray.

The bichromatic waves were simulated by superimposing two sinusoidal wave components with the same heights $H_1 = H_2$ and slightly different periods T_1 and T_2. The water surface elevation η of the grouping wave is expressed by the linear theory as

$$\eta = \frac{H_1}{2}\cos(2\pi t/T_1) + \frac{H_2}{2}\cos(2\pi t/T_2 + \varphi) \tag{1}$$

so that the maximum wave height in the group is $2H_1(= 2H_2)$. Since the energy density is proportional to $\overline{\eta^2}$, the energy density of the grouping wave is proportional to $H_1^2/2$. The equivalent wave height H_e of monochromatic wave with the

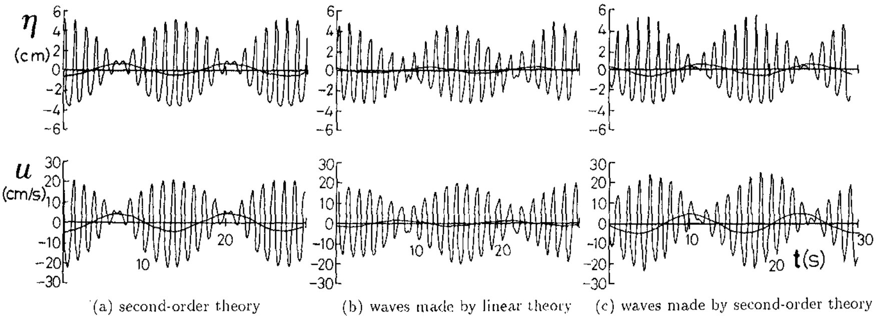

Fig. 2 Surface elevation and near-bottom velocity of bichromatic waves

same energy density as the grouping wave is therefore determined by

$$H_e = \sqrt{2}H_1 \tag{2}$$

The period T_l of the wave group and the mean period T_s of individual short-wave in the group were given as follows:

$$T_l = \frac{T_1 T_2}{|T_1 - T_2|}, \quad T_s = \frac{2T_1 T_2}{T_1 + T_2} \tag{3}$$

The ratio T_l/T_s thus indicates the number of waves in a group. These parameters will be used to analyze laboratory data although nonlinear waves were observed in the flume.

Experiments were performed for 30 runs using non-breaking grouping waves. Eleven runs of experiments were also performed by using monochromatic waves with equivalent wave heights H_e. Experimental conditions as well as measured net sand transport rates were listed in Table 1.

Figure 2 shows an example of water surface elevation η and near-bottom velocity u under a bichromatic grouping wave. Figure 2 (a) shows theoretical time histories estimated by the second-order Stokes wave theory. It is noticed that long waves are induced in such a way that water level decrease and offshore flow are developed under large waves. Figure 2 (b) shows η and u measured under bichromatic waves generated by using the linear wave variation expressed by Eq. (1) as the input to the wave generator. It was noticed that the observed waves by the linear wave input did not reproduce the phase correlation between short- and the bound long-waves well. Figure 2 (c) illustrates η and u where the input signal was simulated by the second-order Stokes wave theory (*e.g.* Mansard and Barthel, 1984). It was found that the desired grouping waves were simulated well as shown in this figure. In the present experiments, the wave generator was controlled by input signals simulated by the second-order Stokes wave theory.

Table 1 Experimental condition and net sand transport rates

(a) monochromatic waves

D(cm)	T(s)	H(cm)	Q(cm^2/s)	
0.02	1.00	7.1	-0.266	$\times 10^{-3}$
0.02	1.00	8.5	-0.523	$\times 10^{-3}$
0.02	1.00	9.9	-0.678	$\times 10^{-3}$
0.02	1.15	7.1	-0.237	$\times 10^{-3}$
0.02	1.15	8.5	-0.917	$\times 10^{-3}$
0.02	1.25	7.1	-0.026	$\times 10^{-3}$
0.02	1.25	8.5	0.934	$\times 10^{-3}$
0.02	1.25	9.9	3.181	$\times 10^{-3}$
0.07	1.25	7.1	0.0	
0.07	1.25	8.5	0.0	
0.07	1.25	9.9	0.369	$\times 10^{-3}$

(b) bichromatic waves

D(cm)	T_1(s)	T_2(s)	H_1, H_2(cm)	Q(cm^2/s)	
0.02	1.00	1.100	5.0	0.176	$\times 10^{-3}$
0.02	1.00	1.175	5.0	1.51	$\times 10^{-3}$
0.02	1.00	1.250	5.0	0.306	$\times 10^{-3}$
0.02	1.00	1.100	6.0	1.59	$\times 10^{-3}$
0.02	1.00	1.175	6.0	3.08	$\times 10^{-3}$
0.02	1.00	1.250	6.0	1.88	$\times 10^{-3}$
0.02	1.15	1.265	5.0	0.359	$\times 10^{-3}$
0.02	1.15	1.351	5.0	0.881	$\times 10^{-3}$
0.02	1.15	1.438	5.0	1.20	$\times 10^{-3}$
0.02	1.15	1.265	6.0	0.584	$\times 10^{-3}$
0.02	1.15	1.351	6.0	2.83	$\times 10^{-3}$
0.02	1.15	1.438	6.0	4.69	$\times 10^{-3}$
0.02	1.25	1.375	5.0	1.71	$\times 10^{-3}$
0.02	1.25	1.469	5.0	0.718	$\times 10^{-3}$
0.02	1.25	1.563	5.0	0.813	$\times 10^{-3}$
0.02	1.25	1.375	6.0	5.12	$\times 10^{-3}$
0.02	1.25	1.469	6.0	3.79	$\times 10^{-3}$
0.02	1.25	1.563	6.0	1.09	$\times 10^{-3}$
0.02	1.25	1.375	7.0	1.67	$\times 10^{-3}$
0.02	1.25	1.469	7.0	3.12	$\times 10^{-3}$
0.02	1.25	1.563	7.0	0.497	$\times 10^{-3}$
0.07	1.25	1.375	5.0	0.111	$\times 10^{-3}$
0.07	1.25	1.469	5.0	0.113	$\times 10^{-3}$
0.07	1.25	1.563	5.0	0.358	$\times 10^{-3}$
0.07	1.25	1.375	6.0	2.87	$\times 10^{-3}$
0.07	1.25	1.469	6.0	2.29	$\times 10^{-3}$
0.07	1.25	1.563	6.0	2.65	$\times 10^{-3}$
0.07	1.25	1.375	7.0	5.11	$\times 10^{-3}$
0.07	1.25	1.469	7.0	3.18	$\times 10^{-3}$
0.07	1.25	1.563	7.0	5.76	$\times 10^{-3}$

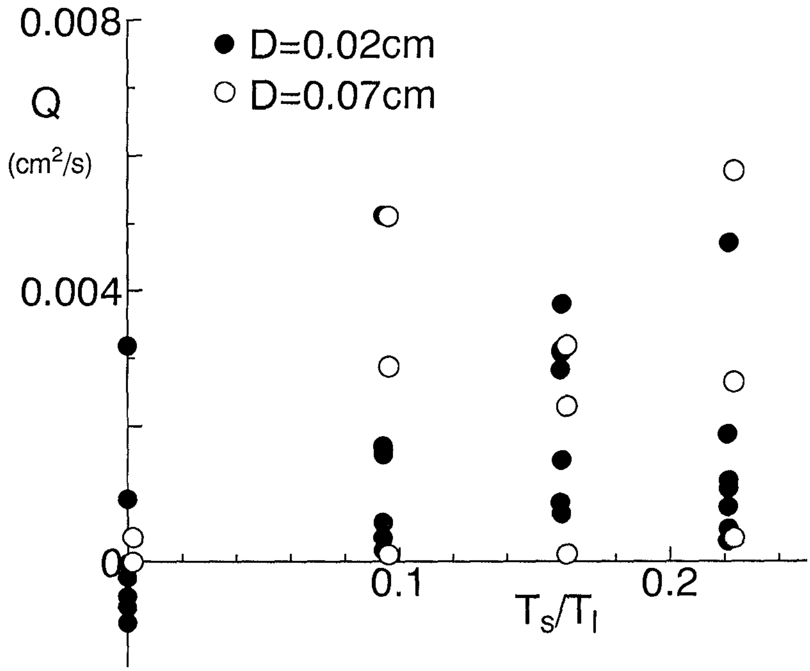

Fig. 3 Measured net sand transport rates

For 0.7mm sand bed, no ripples were developed and sand particles were transported by bed load. Sand particles were observed to be in motion during a few wave period just after the passage of the largest wave in the group. For 0.2mm sand bed, on the other hand, sand ripples were always observed and suspended transport was dominant in all the runs.

Figure 3 shows net sand transport rates measured in all the experimental runs. The positive rates means the onshore transport. The horizontal scale is T_s/T_l, which is the inverse of the number of waves in a group. Data for monochromatic waves are plotted at $T_s/T_l = 0$. The transport direction of coarse sand was always in the onshore direction. Fine sand was also always transported in the onshore direction under grouping waves but the transport direction was offshore in some cases of monochromatic waves. This is because coarse sand was transported by bed load and fine sand was transported primarily by suspended load. Numerical models estimating the net sand transport rate were developed for both bed load and suspended load.

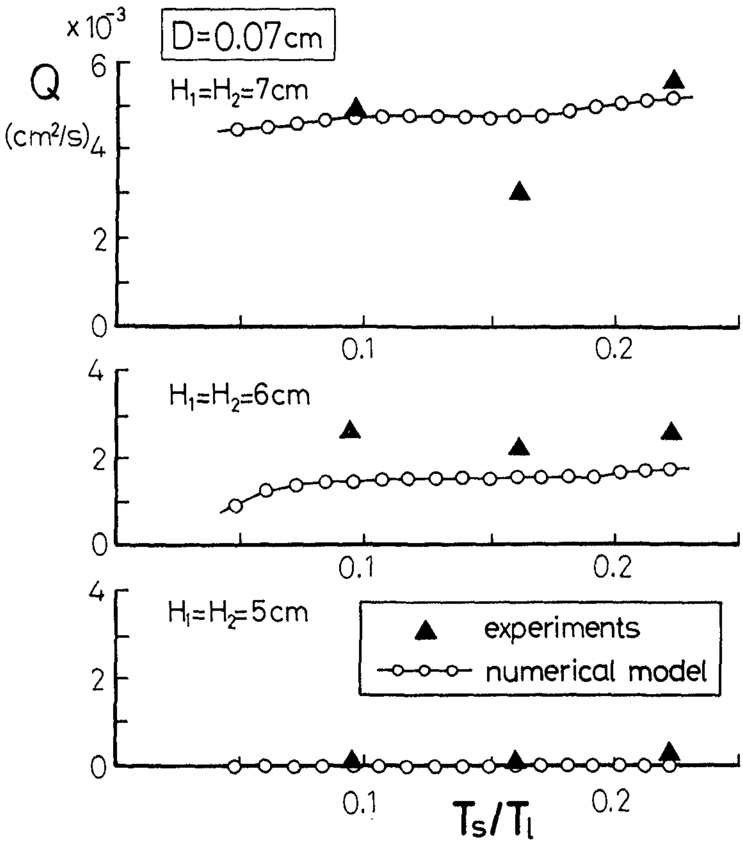

Fig. 4 Net sand transport rates for coarse sand

3. NUMERICAL MODEL

3.1 Bed load

Figure 4 shows net sand transport rates Q for coarse sand. The abscissa T_s/T_l indicates the inverse of the number of waves in a group. The symbol ▲ represents measurement and the solid line indicates a numerical computation in which sand transport rate was computed by a power model expressed by

$$Q = \alpha_b w_s D\overline{(\Psi(t) - \Psi_c)u}/\sqrt{sgD} \tag{4}$$

where $\alpha_b(=1.5)$ was a nondimensional coefficient, w_s the settling velocity of sand particle, $\Psi(t)$ the instantaneous Shields parameter, Ψ_c the critical Shields parameter, s the specific gravity of sand particle in water and g the gravity acceleration.

The overbar indicates taking temporal average over the period of wave group.

The Shields parameter was estimated by using the laminar boundary layer theory since turbulence was observed to be weak in all the experiments with coarse sand. The second-order Stokes wave theory was used to compute velocity variation near the bottom. According to the theory, the velocity variation under a bichromatic wave was expressed by the sum of the first-order components and the second-order components as

$$\begin{aligned} u &= u_1 \cos\sigma_1 t + u_2 \cos\sigma_2 t + u_{12}\cos 2\sigma_1 t + u_{22}\cos 2\sigma_2 t \\ &+ u_{2a}\cos(\sigma_1+\sigma_2)t + u_{2l}\cos(\sigma_1-\sigma_2)t \end{aligned} \tag{5}$$

where $\sigma_1(= 2\pi/T_1)$ and $\sigma_2(= 2\pi/T_2)$ are angular frequencies, u_1 and u_2 are velocity amplitudes of the first-order components and u_{12}, u_{22}, u_{2a}, u_{2l} are velocity amplitudes of the second-order components. Assuming laminar flow in the bottom boundary layer, the bottom shear stress τ is expressed by

$$\begin{aligned} \tau(t) &= \rho\sqrt{\sigma_1\nu}\, u_1\cos(\sigma_1 t+\pi/4) + \rho\sqrt{\sigma_2\nu}\, u_2\cos(\sigma_2 t+\pi/4) \\ &+ \rho\sqrt{2\sigma_1\nu}\, u_{12}\cos(2\sigma_1 t+\pi/4) + \rho\sqrt{2\sigma_2\nu}\, u_{22}\cos(2\sigma_2 t+\pi/4) \\ &+ \rho\sqrt{(\sigma_1+\sigma_2)\nu}\, u_{2a}\cos((\sigma_1+\sigma_2)t+\pi/4) \\ &+ \rho\sqrt{|\sigma_1-\sigma_2|\nu}\, u_{2l}\cos((\sigma_1-\sigma_2)t+\pi/4) \end{aligned} \tag{6}$$

where ρ and ν are the density and the kinematic viscosity of water respectively. The instantaneous Shields parameter is related to the bottom shear stress by

$$\Psi(t) = \tau(t)/(\rho s g D) \tag{7}$$

The value of $\Psi - \Psi_c$ in Eq. (4) was set to be zero when Ψ was smaller than Ψ_c. It was confirmed in **Fig. 4** that the model predicted the onshore transport of coarse sand in a good accuracy.

3.2 Suspended load

For fine sand sand ripples were always observed and suspended sand was dominant above rippled bed. Figure 5 shows the relationship between the ripple wavelength λ and the diameter d_o of water particle displacement near the bottom. The value of d_o was estimated by using the linear wave theory. For grouping waves, d_o was estimated by using energy equivalent wave height H_e and individual wave period T_s, where H_e and T_s are related to the dimensions of the grouping wave by Eqs. (2) and (3). The ripple wavelength under grouping waves was longer than that under monochromatic waves as long as H_e was used as the representative wave height.

Figure 6 shows vertical distributions of time-averaged sand concentrations $\bar{C}$ under a grouping wave and a monochromatic wave with equivalent wave height.

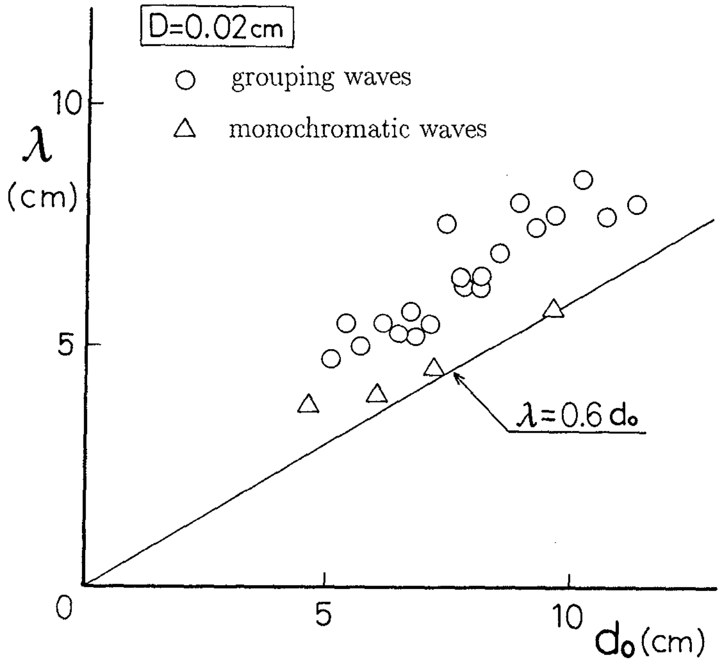

Fig. 5 Wavelength of sand ripples for fine sand

It was found that sand concentration tended to be larger in grouping waves than in monochromatic waves. The eddy diffusivity ε estimated from **Fig. 6** was also larger in grouping waves than in monochromatic waves, which was associated with larger sand ripples observed under grouping waves.

Suspended load was modeled on the basis of the following one-dimensional diffusion equation:

$$\frac{\partial C}{\partial t} = \varepsilon \frac{\partial^2 C}{\partial z^2} + w_s \frac{\partial C}{\partial z} \tag{8}$$

The boundary condition at the bed was described by a pick-up function $p_r(t)$ which simulated intermittent ejection of sand above rippled bed (Nielsen, 1988). The entrainment of sand was assumed to occur at the time of every flow reversal. The time t_i of the i-th flow reversal was determined from the velocity variation simulated by the second-order Stokes wave theory. The boundary condition at the bed was then expressed as follows:

$$\varepsilon \frac{\partial C}{\partial z}|_{z=0} = -p_r(t) = -\sum_i \rho_s \alpha_s w_s D(\Psi_i - \Psi_c) u_i T_i / (\lambda \sqrt{sgD})\ \delta(t - t_i) \tag{9}$$

where α_s(=0.2) was a coefficient, ρ_s was the density of sand particle, T_i, u_i and Ψ_i were the period, the velocity amplitude and the Shields parameter of i-th wave

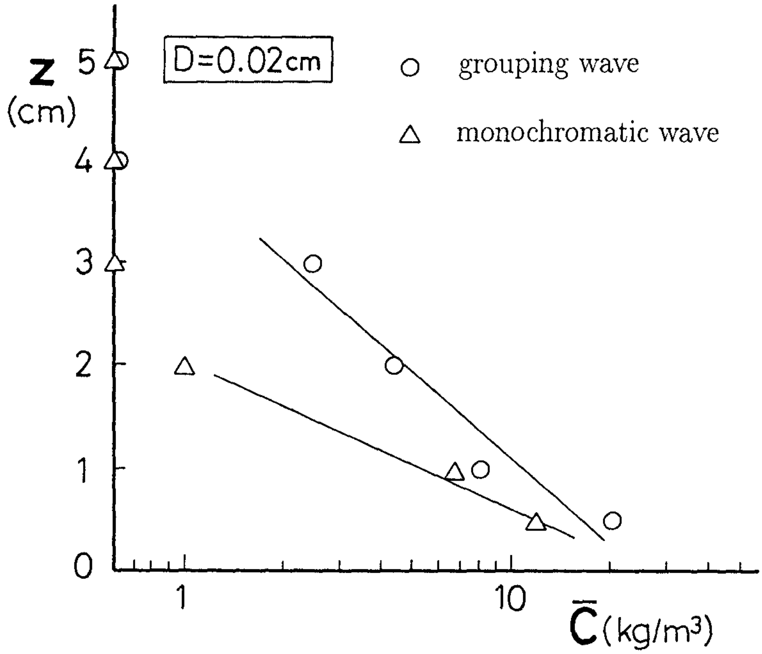

Fig. 6 Vertical distributions of suspended sand concentration

respectively, and $\delta(t)$ was Dirac's delta function. The Shields parameter Ψ_i was estimated by

$$\Psi_i = \frac{f_w u_i^2}{2sgD} \tag{10}$$

where f_w was Jonsson's friction factor. For eddy diffusivity, the following relation proposed by Nielsen (1988) was employed:

$$\varepsilon = w_s \eta (1.24 \exp[-40(w_s/\hat{u}_{1/3})^2] + 0.2) \tag{11}$$

where η was the wave height of observed sand ripples and $\hat{u}_{1/3}$ was the significant amplitude of near-bottom velocity variation.

Figure 7 shows an example of temporal variation of water surface elevation η, near-bottom velocity u and sand concentrations C measured and simulated by the model. Sand concentrations were compared with measurements at elevations z=3cm, 2cm, 1cm, 0.5cm. The long wave component extracted by a numerical low-pass filter was also shown in the figure. It was reproduced in the model that the sand concentration becomes maximum just after the passage of largest wave in the group.

When we integrate the correlation $\overline{Cu}$ at various heights, we can estimate suspended sand flux at the section, which can be compared with net sand transport

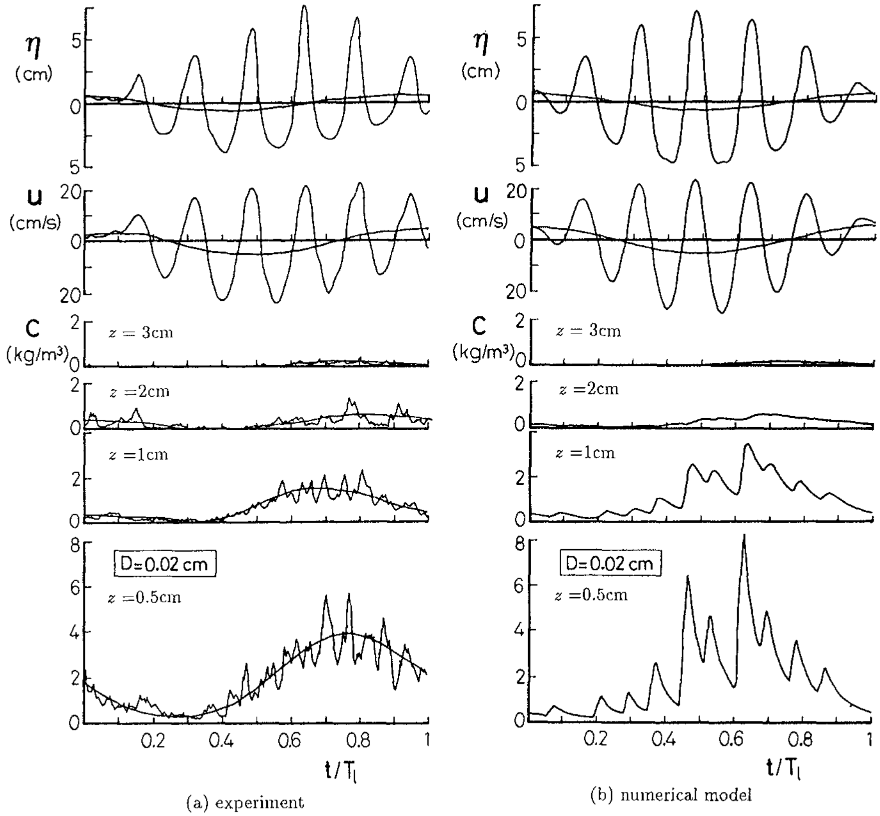

Fig. 7 Comparison of numerical computation with measurements

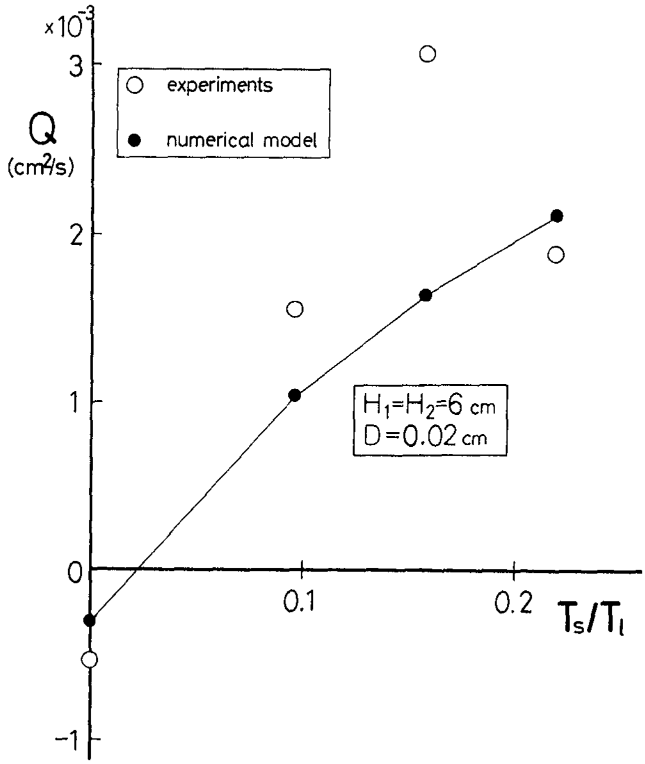

Fig. 8 Comparison of net sand transport rates

rates estimated from the mass difference of sand in sand tray. Figure 8 shows the relationship between the net sand transport rates Q and T_s/T_l. Net sand transport rate under monochromatic wave was plotted at $T_s/T_l=0$. The numerical model based on the diffusion equation reproduced the experimental results that the direction of net sand transport in grouping waves was opposite to that in monochromatic waves. It is also reproduced in the model that the transport rates increased with the decrease of the number of waves in the wave group.

Figure 9 shows co-spectra between C and u for monochromatic wave and grouping wave. The co-spectrum indicates the contribution of each frequency to the total suspended load. There is a sharp peak of offshore transport for monochromatic wave. This is because under shallow water waves propagating over rippled bed, we usually have offshore transport of fine sand since more sand is accumulated in a vortex behind ripple crests during stronger onshore flow and transported offshore after the flow reversal.

Under grouping waves, to the contrary, the contribution at the peak frequency

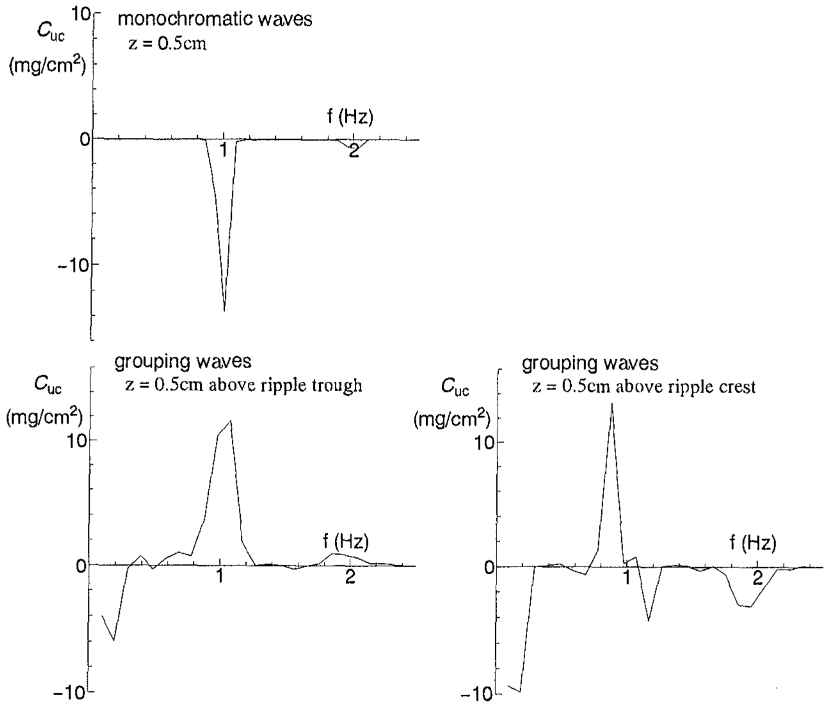

Fig. 9 Co-spectra between u and C

was reversed to onshore transport. It is also noticed that a large contribution to the offshore was observed by long wave component. The reason for the reversal of the contribution at the peak frequency is explained by the asymmetry in the time history of velocity. Since offshore flow is induced by long wave component under large waves, velocity amplitude of offshore flow becomes larger than that of onshore flow. This makes suspended sand cloud created during offshore flow bigger than that during onshore flow, which results in net onshore transport of suspended sand at the peak frequency. The offshore contribution by the long wave component is explained by the same mechanism suggested by Shi and Larson (1984), that is, more sediment will be suspended under large waves which will be transported by offshore flow induced by the bounded long wave. The direction of the total net sand transport under non-breaking grouping waves will be determined by the balance of these two contributions. Net onshore transport of fine sand observed in the present experiments means that the onshore contribution by the short wave component was always larger than the offshore contribution by the long wave component within the range of experiments.

4. CONCLUSIONS

Laboratory experiments showed that the direction of net transport of fine sand was onshore under non-breaking grouping waves although it was offshore under monochromatic waves with equivalent wave height. Laboratory experiments also proved that wave grouping plays an important role in particular for the case in which suspended load is predominant. A numerical model developed on the basis of diffusion equation of sand concentration was confirmed with experiments.

Extension of the model to random wave conditions will be presented in the next opportunity.

REFERENCES

Mansard, E.P.D. and V. Barthel (1984): Shoaling properties of bounded long waves, *Proc. 19th Conf. on Coastal Engineering,* pp. 798-814.

Nielsen, P. (1988): Three simple models of wave sediment transport, *Coastal Engineering,* Vol. 12, pp. 43-62.

Shi, N.C. and L.H. Larson (1984): Reverse sediment transport induced by amplitude-modulated waves, *Mar. Geol.,* 54, pp. 181-200.